

Article

Not peer-reviewed version

DFT Investigation of the Mechanism of Methoxycarbonylation of Styrene by Palladium Chloride

[Shanti Gopal Patra](#)^{*}, [Aritra Saha](#), [Pratim Kumar Chattaraj](#)^{*}

Posted Date: 21 October 2024

doi: 10.20944/preprints202410.1524.v1

Keywords: Methoxycarbonylation; organometallic; Pd catalyst; DFT; EDA-NOCV



Preprints.org is a free multidiscipline platform providing preprint service that is dedicated to making early versions of research outputs permanently available and citable. Preprints posted at Preprints.org appear in Web of Science, Crossref, Google Scholar, Scilit, Europe PMC.

Copyright: This is an open access article distributed under the Creative Commons Attribution License which permits unrestricted use, distribution, and reproduction in any medium, provided the original work is properly cited.

Article

DFT Investigation of the Mechanism of Methoxycarbonylation of Styrene by Palladium Chloride

Shanti Gopal Patra ^{1,*} Aritra Saha ¹ and Pratim Kumar Chattaraj ^{2,*}

¹ Department of Chemistry, National Institute of Technology Silchar, Silchar, 788010, India

² Department of Chemistry, Birla Institute of Technology, Mesra, Ranchi, Jharkhand 835215, India

* Correspondence: pratim.chattaraj@gmail.com (PKC); shanti@che.nits.ac.in (SGP)

Abstract: The alkoxycarbonylation of styrene by palladium chloride is studied employing the density functional theory (DFT). Initially, $[\text{PdCl}_3]^-$ reacts with methanol to form the methoxy-bound intermediate, which undergoes β -hydride elimination to form the key intermediate $[\text{PdCl}_2\text{H}]^-$. Then, a 1,2-insertion reaction to styrene takes place to form linear and branched alkyl coordinated with the Pd^{II} . Then CO coordination followed by a 1,1-insertion reaction leads to the formation of acyl intermediate. Next, the methanolysis leads to the formation of esters. Previous reports with other catalysts suggested the intermolecular/intramolecular transition state (TS) formation with a high activation barrier, and this step was the bottleneck. To the best of our knowledge, it is the first time we have considered a two-step mechanism for the alcoholysis of the ester formation mechanism. After coordination with the metal, the methanol undergoes oxidative addition to form the Pd^{IV} square pyramidal intermediate, followed by reductive elimination to form the ester with regeneration of the metal hydride active intermediate. Deeper insight into the nature of bonding at the TSs is obtained through energy decomposition with natural orbital for chemical valence (EDA-NOCV) and quantum theory of atoms in molecules (QTAIM).

Keywords: Methoxycarbonylation; organometallic; Pd catalyst; DFT; EDA-NOCV

1. Introduction

Carbonylation reaction is the conversion of alkenes or alkynes to aldehydes, acids, esters, or lactones using carbon monoxide in a one-pot synthesis.[1–3] Otto Roelen, while working on the Fischer-Tropsch reaction, first reported the transition metal-catalyzed carbonylation reaction.[1] Transition metals, such as Fe, Co, Ru, Rh, Ir, etc., are utilized as catalysts for carbonylation reactions.[4,5] Along with academic development, many industrial processes are developed based on carbonylation reactions, where CO is considered the C1 feedstock.[4] One such example is the production of Monsanto acetic acid, which starts from methanol and carbon monoxide.[5] In the carbonylation reactions, the use of alkene/alkyne substrate in the presence of water, amine, and alcohol nucleophiles leads to the formation of carboxylic acid, amide, and ester, respectively.[4,6] Due to poor selectivity, the carbonylation of α -olefins leads to various products unless neighboring group participation is involved.[7–11] However, selectivity can be achieved by the use of different ligands[12–19], the use of other additives, and reaction conditions (temperature, CO pressure, etc.).[1,20–23]

In homogeneous catalysis involving β -hydride elimination, oxidative addition, reductive elimination, migratory insertion, and carbon-carbon bond formation, the Pd complexes are significant as their reactivity can be tuned using various ancillary ligands.[10,24,25] One of the vital step-up reactions in organometallic chemistry is carbonylation, which can be achieved by Pd^0 and Pd^{II} with regio and stereoselectivity when the complexes are decorated with suitable phosphine ligands.[26–31] Further, fine-tuning is also achieved by adding a variety of substituents to the phosphorous donor and altering the electronic and steric properties of the complexes.

Previous studies have shown that metal hydride intermediate $[\text{Pd}^{\text{II}}\text{-H}]$ is a key intermediate for the overall transformation under acidic conditions.[32,33] Mehara et al.[34] have summarized the

catalytic cycle where, initially, the alkene undergoes a 1,2-insertion reaction with the $[Pd^{II}-H]$ to form the palladium alkyl with two possibilities in the case of asymmetric alkene. Next, a 1,1-CO insertion reaction forms the acyl-palladium complexes, which have two possibilities. Finally, the alcoholysis leads to the ester formation with regeneration of the vital intermediate $[Pd^{II}-H]$. Various studies were performed in the past to investigate the mechanism, such as the $[Pd^{II}-H]$ was detected through NMR[35–38]; the metal-acyl intermediate was isolated and characterized by X-ray structures[37,39,40]. In addition, chromatography studies such as HPLC, GC-MS,[37,39] deuterium labeling [41], and theoretical studies also confirm the presence of different intermediates.

Another mechanism was proposed where the starting Pd^0 catalyst is oxidized to Pd^{II} by an oxidant, which then reacts with alcohol to form the alkoxy intermediate. Followed by a CO insertion reaction to form the alkoxycarbonyl-Pd intermediate.[42,43] Next, alkene undergoes a 1,2-insertion reaction followed by β -hydride elimination to form the unsaturated ester. Thus, The hydride intermediate releases proton or HCl to form the Pd^0 starting compound via the reductive elimination step. In practice, the formation of the unsaturated esters is not so favourable, especially in the acidic medium where the reductive elimination step is disfavoured.[34] Further, the role of oxidizing agents ($Cu(OAc)_2$, $CuCl_2$) in combination with solvents (acetonitrile, DMF, DMSO) plays an essential role in determining product selectivity. [44]

Several modeling studies of Pd-catalysed alkoxycarbonylation of alkenes and alkynes were summarized in the perspective article by Ahmad et al.[45] With bidentate diphosphine ligands, the hydride pathway is more favorable.[36,39,42,46,47] The final alcoholysis step was the most challenging, finding the more favorable path with the least activation energy barrier. The intramolecular alcoholysis was shown to be unsurmountable, while the intermolecular pathway could achieve the lower activation barrier.[48] Here, we have considered the catalytic methoxycarbonylation of styrene by $[PdCl_3]^-$ in the presence of CO to give linear and branched esters. We have considered the hydride mechanism for the overall catalysis. The most significant change to the mechanism is the final alcoholysis step. The step consists of two sub-steps, where alcohol first undergoes coordination with the metal to form an alcohol-bound complex, which then undergoes oxidative addition to create a Pd^{IV} complex with coordination of hydride, methoxide, and acyl. Next, it undergoes reductive elimination where methoxide and acyl form a sigma bond to form the ester, and Pd^{IV} reduces to Pd^{II} . The free energies of different steps for the formation of branched and linear esters are compared side by side. The energy decomposition analysis with natural orbital for chemical valence (EDA-NOCV) analysis and quantum theory of atoms in molecules (QTAIM) is carried out at the TSs to gain deeper insight into the mechanism.

2. Computational Details

The geometry optimization and frequency calculations for the intermediate and transition state structures are carried out employing the Gaussian 16 Version C1.0.[49] The absence of any imaginary frequency in the intermediate case indicates the presence of true minima, while the presence of strong imaginary frequency implies the transition state structure. Intrinsic reaction coordinate (IRC) calculations for the forward and reverse direction correspond to the corresponding product and reactant, respectively. For all types of calculations, the PBE0[50,51] functional (using the keyword PBE1PBE) was used unless otherwise specified. Optimization and frequency calculations are performed using LanL2DZ[52] basis set for the Pd atom and 6-31+G(d,p) Pople's basis set for the H, C, O, and Cl atoms. This combined basis is denoted as bs1. At the optimized geometry, single-point calculations are performed employing the SDD[53,54] basis set for the Pd atom and 6-311+G(d,p) Pople's basis set for the H, C, O, and Cl atoms. This combined basis is denoted as bs1. The solvation effect in methanol solvent was taken into consideration using the solvation molecular dynamics model (SMD).[55] Thus, the final level of the theory of thermochemistry becomes SMD/PBE0/bs2. To incorporate the zero-point corrections to the free energies at the SMD/PBE0/bs2, the corresponding zero-point correction is taken from the PBE0/bs1 level of theory. In the solvation process, molecules are transformed from the gas phase (1 atm) to the condensed phase (1 M), and hence, a concentration correction of $\Delta G^{0 \rightarrow *}=1.89 \text{ kcal mol}^{-1}$ was applied to the free energy values.[56–58] Quantum theory of atoms in molecules (QTAIM) and electron localization function (ELF) analyses were performed using the Multiwfn software.[59] Energy decomposition analysis (EDA) was performed at the B3LYP-D3(BJ)/TZ2P level of theory on the optimized geometries using the sobEDA[60] method implemented

in the Multiwfn program.[59] Grimme's dispersion correction (GD3)[61] with Becke-Johnson parameters[62] was incorporated in the EDA calculations. Extended transition state natural orbital for chemical valence (ETS-NOCV) is performed using the Multiwfn program.

3. Results and Discussion

The general mechanistic path of the formation of ester starting from the $[\text{PdCl}_3]^-$ (**int1**), CO, styrene, and methanol proceeds through the following steps: first methanol reacts with $[\text{PdCl}_3]^-$ to form $[\text{PdCl}_2(\text{OCH}_3)]^-$ (**int2**) with the release of HCl. This step is found to be endergonic with $\Delta G = 14.1 \text{ kcal mol}^{-1}$. Next, the hydrogen atom attached to the methyl group undergoes β -hydride elimination through the transition state **TS1** (Figure 1). This form the metal hydride intermediate $[\text{PdCl}_2\text{H}]^-$ and formaldehyde. The free energy of activation is calculated to be $-1.22 \text{ kcal mol}^{-1}$, which is significantly less activation energy, implying the reaction's feasibility.[6] At the TS1, the bond lengths are Pd-O, 2.121; Pd-H, 1.542; C-H, 1.957 Å. Here, the C-H bond is cleaved, the Pd-H bond is formed, and the C-O bond transforms from single to double. The hydride intermediate $[\text{PdCl}_2\text{H}]^-$ formed is the active catalyst in the catalytic cycle. This cycle has the following steps: i) styrene attacks the **int3** to form an alkyl-bound Pd complex. Now, in this step, the metal-bound hydride undergoes insertion into the alkene double bond in two possible ways (Scheme 1): a) the hydride attacks the phenyl substituted part of the alkene (**cycle 1**) through the formation of transition state **TS2**, or b) it can attack the unsubstituted part of the alkene (**cycle 2**) through the formation of transition state **TS2a**. Here, the alkyl-bound intermediates **int4** or **int4a** are formed. Let us first elaborate on the mechanism considering the **cycle 1**. ii) The CO reacts with the alkyl bound intermediate **int4** via coordination of CO ligand to the Pd metal to form the intermediate **int5**. iii) Next, CO insertion reaction takes place to form the intermediate **int6** via the transition state formation **TS3**; iv) the methanol undergoes coordination to the free site of **int6** to form the methanol, bound intermediate **int7**; iv) the methanol bound intermediate undergoes oxidative addition via **TS4** to form the methoxide and hydride bound Pd^{IV} complex (**int8**); vi) finally, the intermediate undergoes reductive elimination via **TS5** to form the methyl ester compound and the active catalyst **int3**. **Cycle 2** is similar to **cycle 1**, but the cycle starts with hydride insertion to the less substitute part of the styrene to form **int4a**. Thereafter, the naming of the intermediates and the transition states are the same, with the addition of 'a' to the names of **cycle 1**.

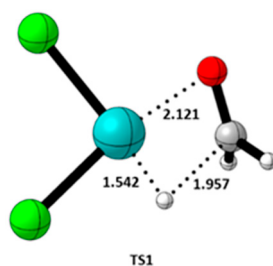
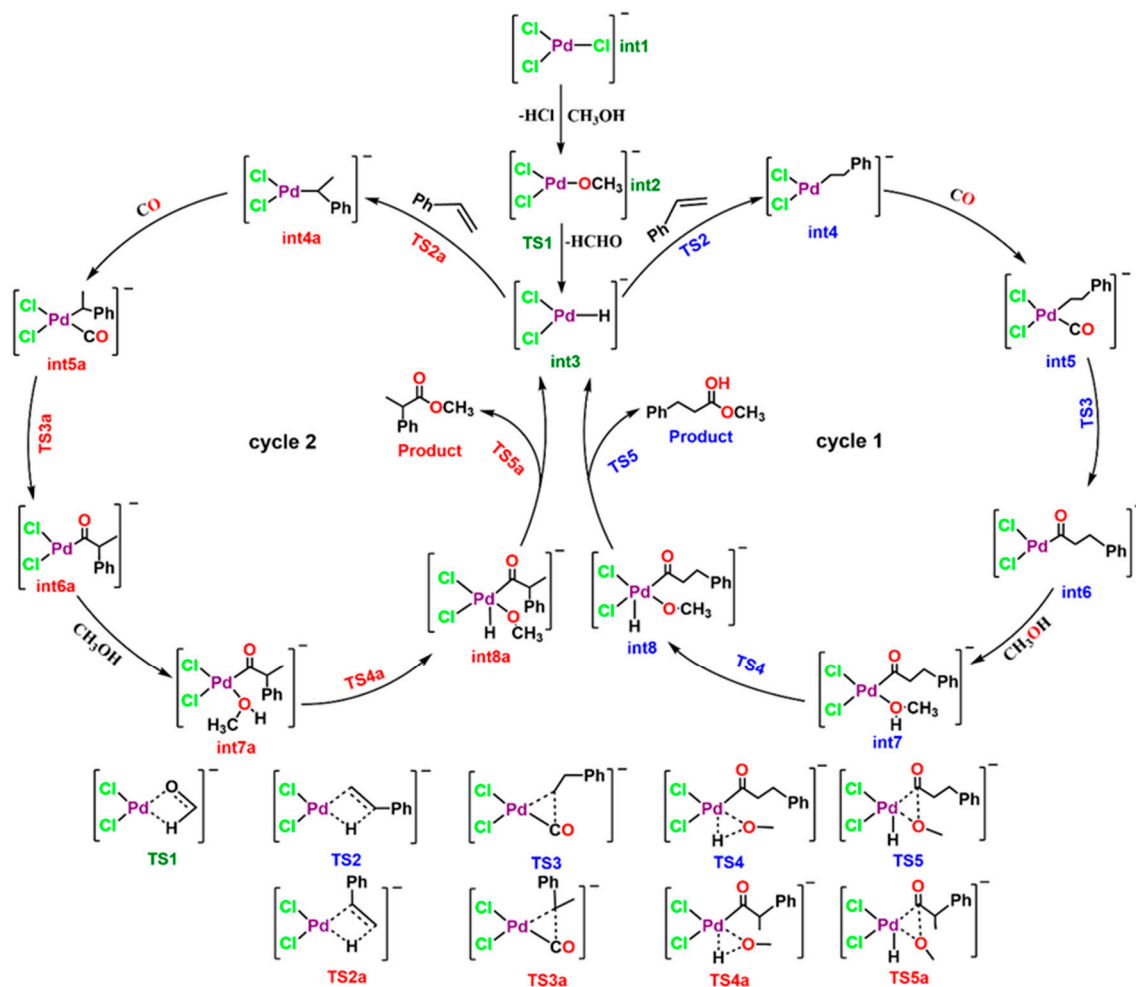


Figure 1. The transition state structure of **TS1**, i.e., β -hydride elimination step. The geometry optimization is carried out at the PBE0/bs1 level of theory.



Scheme 1. Catalytic cycles involving various transition states in intermediates for the $[\text{PdCl}_3]^-$ -catalyzed alkoxycarbonylation of styrene in the presence of CO in methanol solvent.

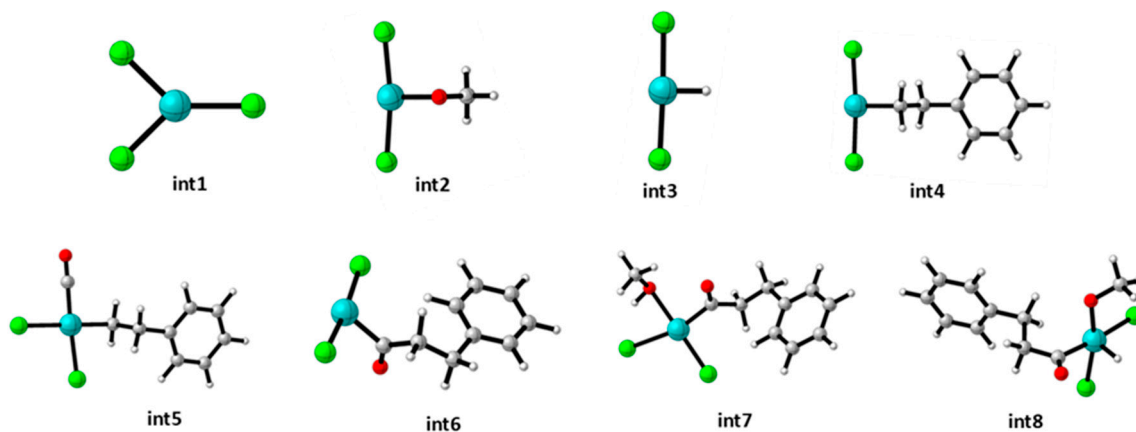


Figure 2. The intermediate structure of **int1-int8** in **cycle1**. The geometry optimization is carried out at the PBE0/bs1 level of theory. Color code: H, white; C, grey; O, red; Cl, green; Pd, cyan.

We have calculated the geometry optimization frequency of the intermediates and transition state structures for both cycles (Scheme 1). The intermediate and TS structures of **cycle 1** are shown in Figures 2 and 3, respectively. For **cycle 2** the respective structures of the intermediates and TSs are given in Figures S1 and S2 of the supplementary information file.

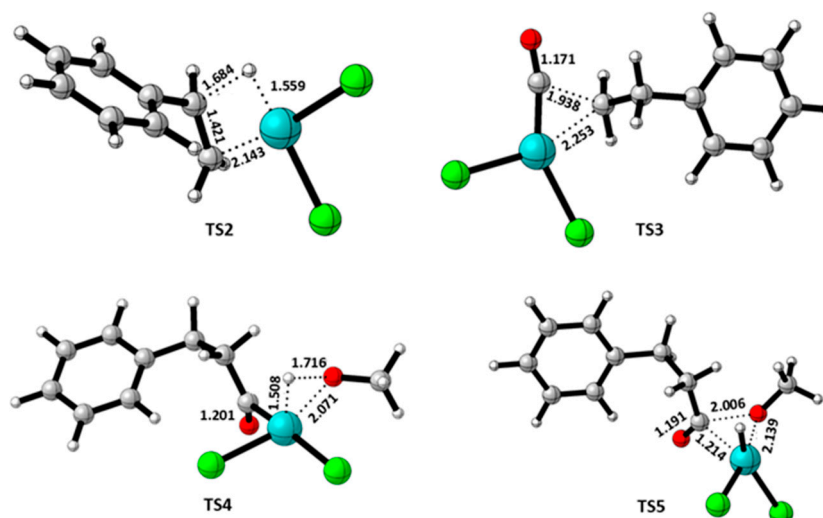


Figure 3. The transition state structure of TS2-TS5 in cycle 1. The geometry optimization is carried out at the PBE0/bs1 level of theory. Colour code: H, white; C, grey; O, red; Cl, green; Pd, cyan.

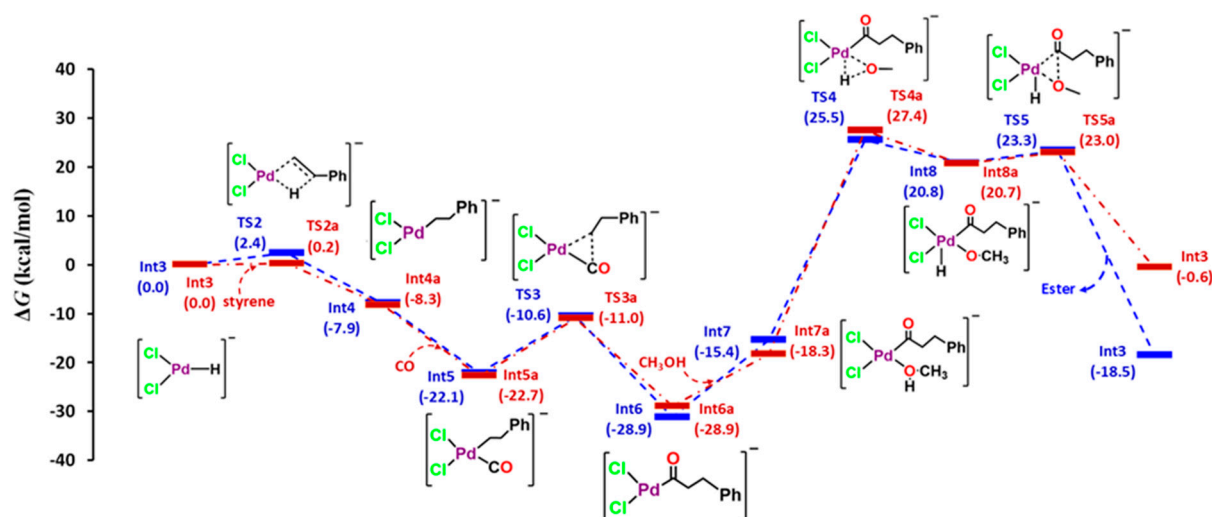


Figure 4. Free energy profile diagram of $[\text{PdCl}_2\text{H}]^-$ catalyzed alkoxy carbonylation of styrene in the presence of CO in methanol solvent. The parentheses values represent the intermediates' relative free energy values and transition states in kcal mol⁻¹. The calculation is carried out at the SMD/PBE0/bs2//PBE0/bs1 level of theory. The intermediates and TSs structures of cycle 1 is shown along the energy profile diagram.

The free energy profile diagram of the formation of different intermediates and TSs is shown in Figure 4. In **cycle 1** the hydride of **int3** attacks at the phenyl substituted part of the styrene to give the phenyl ethyl coordinated intermediate **int4**. The reaction proceeds through the formation of a **TS2** intermediate with an activation-free energy barrier of 2.40 kcal mol⁻¹. The activation barrier is comparable to the recent report of similar reactions starting from propene using substituted phosphine-coordinated Pd complexes.[16] In **cycle 2**, the reaction is similar, but hydride attacks at the less substituted part of styrene to form intermediate **int4a**. The reaction proceeds with the formation of **TS2a** with an activation energy barrier of only 0.24 kcal mol⁻¹. Thus, the branched alkyl formation is more favorable for the hydride insertion step. In the **TS2/TS2a**, the bond lengths are Pd-C, 2.143 (2.231); Pd-H, 1.559 (1.553); C-H (1.704), 1.684; and C-C, 1.421 (1.417) Å. The bond lengths are very much comparable. In the next step in **cycle 1**, CO gets coordinated to the vacant site to form **int5**. The CO coordination is found to be exergonic with $\Delta G = -14.26$ kcal mol⁻¹. The same reaction in **cycle 2** proceeds with $\Delta G = -14.49$ kcal mol⁻¹ to form intermediate **int5a**. Then, in **cycle 1**, the PhCH_2CH_2 group undergoes an insertion reaction to the CO to form the intermediate **int6**. In the transition state, **TS3**, the PhCH_2CH_2 started forming a bond with the carbon atom of CO with an activation-free

energy barrier of 11.55 kcal mol⁻¹. In the case of **cycle 2**, in a similar reaction, the bond is formed between the carbon atom of CO and the carbon atom of the PhCH₃CH group. The reaction proceeds through the formation of **TS3a** with an activation barrier of 11.77 kcal mol⁻¹. It is important to note that not much difference in the activation barrier is observed in the CO insertion step. These activation barriers also correspond well with the previous report.[16] At the **TS3/TS3a**, the bond lengths are Pd-C, 2.253 (2.321); C-C, 1.938 (1.951); C-O, 1.171 (1.167) Å. The Pd-C bond length in **TS3** is shorter than that of **TS3a**. This is because of the presence of methyl group in Ph(CH₃)CH in **TS3a**, which increases the steric hindrance and eventually increases the barrier of CO insertion reaction of the C-C bond. However, the C-O bond length of carbonyl is shorter in **TS3a**, as the attack of alkyl is less close than in **TS3**.

Next, methanol is coordinated to the vacant site of the three coordinated intermediate **int6** to form the four coordinated intermediate **int7** and **int7a** for cycles **1** and **2**, respectively. Next, methanol undergoes oxidative addition to form the Pd^{IV} intermediates **int8/int8a**, respectively. The reaction proceeds through the formation of transition states **TS4/TS4a** with an activation-free energy barrier of 40.89 and 45.74 kcal mol⁻¹, respectively. Approximately 5 kcal mol⁻¹ higher activation barrier for the branched acyl group suggests that linear ester formation is more favorable. At the **TS4/TS4a**, the bond lengths are Pd-O, 2.071 (2.074); Pd-H, 1.508 (1.513); O-H, 1.716 (1.688); C-O, 1.201 (1.201) Å. This requires the highest activation barrier and is the rate-determining step. Next, **int8/int8a**, the OCH₃ group, and PhCH₂CH₂CO/Ph(CH₃)CHCO group undergo coupling via reductive elimination to form the intermediates **int9/int9a**. The reactions proceed via **TS5/TS5a** with an activation-free energy barrier of 2.52/2.32 kcal mol⁻¹. The difference is minimal, and the shallow activation barrier suggests the feasibility of the step. However, considering the free energy values, the linear ester is stable by 18 kcal mol⁻¹ compared to the breached one. At the **TS5/TS5a**, the bond lengths are Pd-O, 2.139 (2.061); Pd-C, 2.214 (2.041); C-O, 2.006 (2.010); C-O, 1.191 (1.191) Å. The decreased C-O bond length between methoxy O and acylium C implies more substantial bond formation and feasibility. This is also supported by the increased Pd-O and Pd-C bond lengths in **TS5**.

At the methanolysis step, Walther et al. reported an activation barrier of ~37.5 kcal mol⁻¹. [63] for the methoxycarbonylation of *cis*-3-hexene using Pd^{II} catalysts coordinated by 1,2-bis((dimethylphosphanyl)methyl)benzene (**DMBPX**) ligand at the B3LYP/TZVP/LANL2DZ//B3LYP/6-31G*/LANL2DZ level of theory. For the intramolecular methanolysis step in methoxycarbonylation of methyl 4-heptenoate with the Pd-**DTBPX** (where **DTBPX** = 1,2-bis(di-*tert*-butylphosphino-methyl)benzene), the overall barrier of 29.1 kcal mol⁻¹ was reported by Roesle et al. [64] at the B3LYP/6-31G*/LANL2DZ level of theory. For the Pd-**DTBPX** catalyzed methoxycarbonylation of ethene overall barrier of ~42.4 kcal mol⁻¹ at the B3PW91-D3/TZVP/LANL2DZ/SMD level of theory associated with the methanolysis step. [65] However, the same study with 1,1'-bis(*tert*-butyl(pyridin-2-yl)phosphanyl)ferrocene ligand leads to the activation barrier of ~30.2 kcal mol⁻¹. Thus, the ligand framework is crucial in decreasing the activation barrier. Jameel *et al.* [65] with 10-undecenoate reported an overall barrier of ~40.0 kcal mol⁻¹ applying the energy span model. So, we can see that without having any better chelating ligand, we got the barrier height of 40.9 and 45.7 kcal mol⁻¹ for the oxidative addition of methanol. Thus, it may be speculated that better bidentate ligands may decrease the activation barrier, which is the subject of further studies.

3.1. Energy Decomposition Analysis (EDA) and Natural Orbital for Chemical Valence (NOCV) Analysis

Next, the energy decomposition analysis is carried out on the transition state structure of the TSs. The fragments considered for the TSs are given in Table 1. At the transition state structures, the energy decomposition analysis considers the two fragments (the details of the fragmentation scheme at different TSs are given in Table 1). The total interaction energy (ΔE_{tot}) is dissected into electrostatic (ΔE_{els}), exchange (ΔE_{x}), repulsion (ΔE_{rep}), orbital (ΔE_{orb}), DFT correlation (ΔE_{DFTc}), and dispersion correction (ΔE_{dc}). The values of total interaction energy and contributions from different components are given in Table 2.

Table 1. The fragmentation scheme used in the energy decomposition analysis (EDA) at the different TSs of **cycle 1** and **cycle 2**. The values in parentheses represent the charge and multiplicity.

TS	fragment1 (charge, multiplicity)	fragment2 (charge, multiplicity)
TS1	HCHO (0, 1)	[PdCl ₂ H] ⁻ (-1, 1)
TS2	styrene (0, 1)	[PdCl ₂ H] ⁻ (-1, 1)
TS3	PhCH ₂ CH ₂ (-1, 1)	[PdCl ₂ CO] (1, 1)
TS3a	PhCH ₃ CH (-1, 1)	[PdCl ₂ CO] (1, 1)
TS4	CH ₃ O (-1, 1)	[PdCl ₂ H(PhCH ₂ CH ₂ CO)] (-1, 1)
TS4a	CH ₃ O (-1, 1)	[PdCl ₂ H(PhCH ₂ CH ₂ CO)] (0, 1)
TS5	CH ₃ O (-1, 1)	[PdCl ₂ H(PhCH ₂ CH ₂ CO)] (0, 1)
TS5a	CH ₃ O (-1, 1)	[PdCl ₂ H(Ph(CH ₃)CHCO)] (0, 1)

Table 2. EDA Analysis at the transition state **TS1-TS5** and **TS2a-TS5a**, where the fragmentation scheme is provided in Table 1. The values in the parenthesis represent their % contribution to the total interaction energy. The calculations are performed at the PBE0- /bs2//PBE0/bs1 level of theory. The energy values are given in kcal mol⁻¹ units.

Species	ΔE_{els}	ΔE_{ex}	ΔE_{pauli}	ΔE_{orb}	ΔE_{cor}	ΔE_{disp}	ΔE_{tot}
TS1	-80.69 (15.94)	-74.23 (14.66)	237.05 (46.83)	-96.98 (19.16)	-13.96 (2.76)	-3.32 (0.66)	-32.13
TS2	-114.29 (16.19)	-110.50 (15.66)	334.23 (47.36)	-120.89 (17.13)	-18.41 (2.61)	-7.44 (1.05)	-37.30
TS2a	-139.13 (16.96)	-115.37 (14.06)	339.21 (41.34)	-198.12 (24.15)	-20.95 (2.55)	-7.67 (0.93)	-142.04
TS3	-192.66 (19.43)	-127.78 (12.88)	428.82 (43.24)	-217.37 (21.92)	-17.76 (1.79)	-7.35 (0.74)	-134.10
TS3a	-150.09 (18.45)	-104.53 (12.85)	349.35 (42.94)	-182.29 (22.41)	-17.34 (2.13)	-9.98 (1.23)	-114.89
TS4	-117.12 (20.96)	-74.31 (13.30)	224.62 (40.20)	-123.04 (22.02)	-14.60 (2.61)	-5.10 (0.91)	-109.55
TS4a	-118.40 (20.60)	-77.01 (13.40)	232.37 (40.42)	-125.94 (21.91)	-15.45 (2.69)	-5.67 (0.99)	-110.12
TS5	-132.38 (21.63)	-81.59 (13.33)	253.06 (41.35)	-122.41 (20.00)	-16.50 (2.70)	-6.02 (0.98)	-105.83
TS5a	-130.04 (21.36)	-81.38 (13.37)	252.20 (41.43)	-121.77 (20.01)	-16.83 (2.76)	-6.46 (1.06)	-104.27

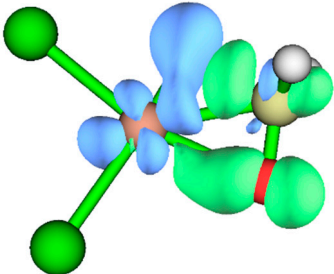
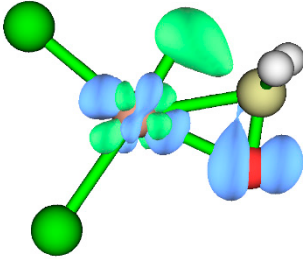
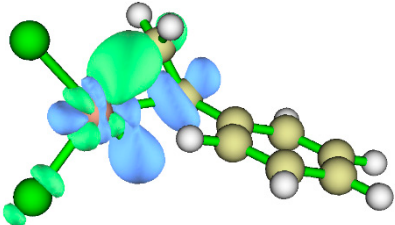
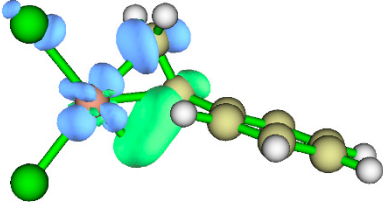
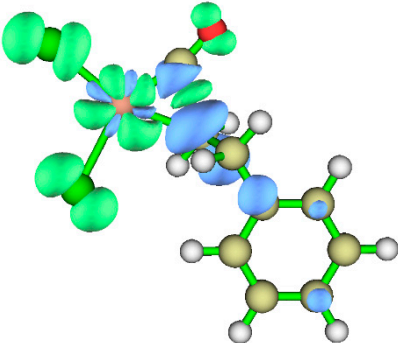
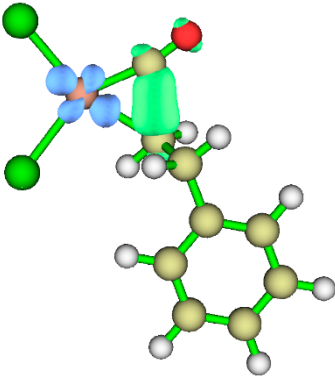
In the **TS1**, considering the [PdCl₂H]⁻ and HCHO fragments, the total interaction energy is calculated to be $\Delta E_{\text{tot}} = -32.13$ kcal mol⁻¹. At this stage, the hydrogen atom transfers from the methyl group to the Pd center. The maximum contribution comes from the orbital part with $\Delta E_{\text{orb}} = -96.98$ (19.16%) kcal mol⁻¹. Other major contributing factors are ΔE_{els} and ΔE_{ex} , with % contributions of 15.94 and 14.66, respectively. Further, the NOCV analysis shows that the most significant contributions come from the first two pairs. These NOCV pair densities are shown in Table 3. The % contributions of pairs 1 and 2 are 63.5 and 22.8, respectively. In both the orbitals, the transfer of electrons from the hydride to the metal can be seen. In **TS3** and **TS3a**, total interaction energies are -134.10 and -114.89 kcal mol⁻¹. In this step, the insertion of the R group (PhCH₂CH₂ or Ph(CH₃)CH) into the CO occurs. Here, the activation energies are comparable. In this step, the maximum contribution comes from the orbital part with a % of ~22, as here, the R⁻ group forms a bond with the CO moiety. A significant number of contributions also comes from the electrostatic, with % contributions of 19.4 and 18.4, respectively. Notably, a covalent bond is formed between the R and CO moieties; hence, the orbital part is higher. At the same time, here, R is nucleophilic type while the CO is nucleophilic type; therefore, the interactions are of electrostatic type. Thus, the electrostatic contribution is also comparable to the orbital part. In the NOCV analysis, the contributions from pairs 1 and 2 are 74.8 and 9.7 %, respectively, in **TS3**. Similar contribution terms can also be seen in TS3a. The first NOCV pair represents the formation of a covalent σ bond between the carbon atoms of PhCH₂CH₂/Ph(CH₃)CH and CO, and the second one is the transfer of electrons from the formed σ bond to the metal center.

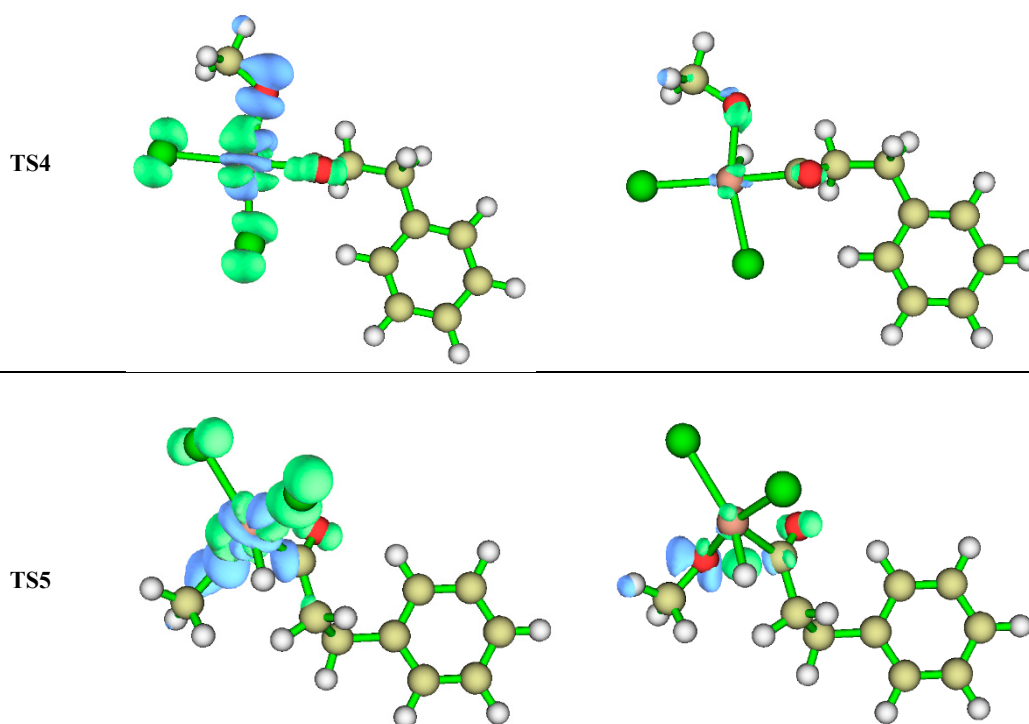
In **TS4** and **TS4a**, the total interaction energies are -109.55 and -109.55 kcal mol⁻¹. The maximum contributing factors here are orbital and electrostatic, with % contributions of ~22 and ~21 for both the TSs. It is important to note that methanol's oxidative addition occurs at this stage. Here, Pd^{II} oxidizes to Pd^{IV}, and at the same time, 2e is transferred to methanol to form methoxide and hydride. Thus, two bonds are formed here between Pd and CH₃O⁻ and H⁻. Also, significant electrostatic interactions operative between positively charged Pd^{IV} and negatively charged CH₃O⁻ and H⁻.

Although the total interaction energies are similar, the activation barrier to form **TS4a** is almost ~ 5 kcal mol $^{-1}$ more than that of **TS4**. This is because of the steric factors that arise with the Ph(CH $_3$)CH group in **TS4a** but not the PhCH $_2$ CH $_2$ group in **TS4**.

In **TS5** and **TS5a**, the total interaction energies are -105.83 and -109.55 kcal mol $^{-1}$. Here, the orbital electrostatic contributions are $\sim 20\%$ and $\sim 22\%$, respectively. In this TS, a covalent bond is formed between OCH $_3$ and PhCH $_2$ CH $_2$ CO/Ph(CH $_3$)CHCO; at the same time, an electron is transferred from negatively charged $^-$ OCH $_3$ and PhCH $_2$ CH $_2$ CO/Ph(CH $_3$)CHCO $^-$ to Pd IV to complete the reductive elimination. Due to the increased charge on Pd, the electrostatic contribution is the maximum. In the NOCV analysis, the σ bond formation between $^-$ OCH $_3$ and PhCH $_2$ CH $_2$ CO/Ph(CH $_3$)CHCO $^-$ and NOCV pairs 1 and 2 contribute ~ 56 and 20% in each TS.

Table 3. The first two most contributing NOCV pairs of the extended transition state are natural orbital for chemical valence analysis at an isosurface value of 0.005 a.u. The green and blue isosurfaces represent the accumulation and depletion of electron density. The calculations are performed at the B3LYP-D3(BJ)/6-311+G(d,p)//PBE0/bs1 level of theory.

TS	NOCV pair 1	NOCV pair 2
TS1		
TS2		
TS3		



3.2. Quantum Theory of Atom in Molecule (QTAIM) Analysis

The nature of the chemical bond and some quantitative aspects regarding chemical bonds is obtained through the application of quantum theory of atoms in molecules (QTAIM).[66–68] The theory provides insight into a molecule's topological distribution of electron density. A point exists Between two atoms where the value of electron density is maximum, called the bond critical point (BCP). Some other critical points are the ring critical point (RCP) and cage critical point (CCP). From the values of different parameters such as electron density ($\rho(r)$), Laplacian of electron density ($\nabla^2\rho(r)$), kinetic energy density ($G(r)$), potential energy density ($V(r)$), total energy density ($H(r)$), electron localization function (ELF), and the second eigenvalue of the Hessian matrix (λ_2) the nature of chemical bonding can be understood.[69–71]

A high value of $\rho(r)$ with the negative sign of $\nabla^2\rho(r)$ implies a strong covalent bond, while a low value of $\rho(r)$ with the positive sign of $\nabla^2\rho(r)$ implies weak interactions.[69,72] To delve deeper into the nature of bonding, the Laplacian of the electron density ($\nabla^2\rho(r)$) is analyzed. This Laplacian is decomposed along the three principal axes, with λ_i representing the eigenvalues of the electron-density Hessian matrix. The sum of these eigenvalues equals $\nabla^2\rho(r)$ (Equation 1):

$$\nabla^2\rho = \lambda_1 + \lambda_2 + \lambda_3 \quad (\lambda_1 \leq \lambda_2 \leq \lambda_3) \quad (1)$$

When two eigenvalues are negative and one is positive ($\lambda_1 < 0$, $\lambda_2 < 0$, $\lambda_3 > 0$), this typically indicates the presence of bonded atomic pairs. A positive Laplacian suggests weaker non-covalent interactions. Negative values of λ_2 , particularly when accompanied by a negative Laplacian, often signify bonding interactions. Hydrogen bonding in water is a classic example. The sign of the Laplacian determines the nature of the interaction: negative denotes attraction, while positive denotes repulsion. It's important to note that the absence of a bond critical point (BCP) does not necessarily mean the absence of weak interactions. From the values and sign of different energy terms at the BCPs, the bonding is understood as covalent bonds, typically characterized by high $G(r)$, negative $V(r)$, $V(r)/G(r) \approx -1$; ionic bonds, often associated with lower $G(r)$, negative $V(r)$, $V(r)/G(r) \approx -2$, and weak interactions, typically characterized by lower $G(r)$, positive $V(r)$, $V(r)/G(r)$ values closer to 0, and lower ρ at BCPs compared to covalent bonds.[69,72]

Values of all these parameters at the TS structures of the forming and breaking bonds are summarized in Table 4. Molecular structure showing the BCP and bond paths are shown in Figures S3-S5. At the **TS1**, the C-H bond is cleaved while the Pd-H bond is formed. Here, the values of $\rho(r)$ are low while the $\nabla^2\rho(r)$ is positive, implying weak interactions. However, the values of $G(r)$ are positive, $V(r)$ is positive, and $-1 < V(r)/G(r) < 0$, and hence it is in between covalent and weak interactions.

On the other hand, a negative value of λ_2 suggests covalent characteristics. The Pd-H bond is cleaved at the **TS2/TS2a**, and the C-H bond is formed. Here, the trend in the values is similar, and clearly, the bonding property is between covalent and weak interaction types, i.e., a weak covalent bond. It is important to note that here, the C-C bond transforms from double to single and is purely covalent. Thus, here it is seen that $\nabla^2\rho(r)$ is negative. In **TS3/TS3a**, the C-C bond is formed between CO and alkyl, and a clear indication of its covalent nature can be seen as $\nabla^2\rho(r)$ is negative with a high value of $\rho(r)$. In addition, weak C-H...Cl type interaction is also observed where the C-H comes from the phenyl ring. In the **TS4/TS4a**, i.e., the oxidative addition step, weak interactions of the type C-H...Cl and C-H...O can be seen where the C-H comes from both the phenyl ring and methyl group. The Pd-H and Pd-O bonds are clearly covalent types, and their values for different parameters are not listed in Table 4. At the **TS5/TS5a**, the O-C bond is formed between methoxide and acyl moiety through reductive elimination. Here, the nature of the O-C bond is weakly covalent. Along with some weak interactions of the type C-H...O (C-H from phenyl), weak H...H type interactions are also observed.

Table 4. Various descriptors are obtained from the quantum theory of atoms in molecules (QTAIM) calculations in the transition state structures of the two pathways involving the bond critical point (BCPs) of the concerned non-covalent interactions. The calculations are performed at the PBE0/bs2 level of theory.

TS	Distance (Å)	bond	$\rho(r_c)$	$\nabla^2\rho(r_c)$	$G(r_c)$	$V(r_c)$	$H(r_c)$	ELF	λ
TS1	1.957	C-H	0.3008	0.1226	0.1235	-0.2163	-0.0928	0.6343	-0.3008
TS1	1.542	Pd-H	0.1369	0.0699	0.0985	-0.1795	-0.0810	0.5295	-0.1369
TS2/	1.683/	C-H	0.3091/	0.0907/	0.1239	-0.2253/	-0.1013/	0.6532/	-0.3091/
TS2a	1.704		0.0823	0.0419	0.0359	-0.0613	-0.0254	0.6076	-0.0823
TS2/	1.558	Pd-H	0.1418/	0.0625/	0.1022/	-0.1889/	-0.8664/	0.5397/	-0.1418/
TS2a	1.553		0.1442	0.0513	0.1020	-0.1912	-0.0892	0.5548	-0.1442
TS2/	1.421	C-C	0.2896/	-0.7424	0.0984/	-0.3825	-0.2840	0.9317	-0.2896
TS2a	1.417		0.2923	-0.7560	0.0981	-0.3855	-0.2873	0.9341	-0.2923
TS2a	2.164	Pd-C	0.0890	0.2540	0.0862	-0.1090	-0.0227	0.2586	-0.0890
TS2/	2.076	Pd-C	0.1045/	0.2010/	0.0865/	-0.1229/	-0.0363/	0.3713/	-0.1045/
TS2a	2.122		0.0947	0.2143	0.0825	-0.1114	-0.0289	0.3197	-0.0947
TS3	3.321	Cl-H(Ph)	0.0456	0.11813	0.0241	-0.0187	0.01962	0.1460	-0.0456
TS3/	1.911/	C-C	0.0405/	-0.0663/	0.1452/	-0.3070/	-0.1618/	0.7724/	-0.1102/
TS3a	1.951		0.1026	-0.1231	0.1335	-0.2754	-0.1419	0.7599	-0.1026
TS4	2.801/	Cl-	0.1091/	0.0843/	0.0628/	-0.0482/	0.0145/	0.1421/	-0.1091/
TS4a	2.847	H(Ph)	0.0520	0.2001	0.0433	-0.1345	0.0245	0.1438	-0.0520
TS4	2.820/	Cl-	0.0377/	0.1351/	0.1008/	-0.0777/	0.0231/	0.1230/	-0.0377/
TS4a	2.852	H(CH ₃)	0.1131	0.0987	0.0730	-0.0555	0.0175	0.1193	-0.1131
TS4a	2.315	H-O	0.0377	0.1413	0.1052	-0.0808	0.0243	0.1130	-0.0377
TS5	2.343/	O-H(Ph)	0.0444	0.1488	0.1179	-0.0993	0.0185	0.1541	-0.0445
TS5a	2.561		0.1228	0.1277	0.0972	-0.0774	0.0198	0.0893	-0.1228
TS5	2.011	H-H	0.0419	0.1381	0.1063	-0.0859	0.0204	0.1553	-0.0419
TS5a	2.031		0.0429	0.1381	0.1064	-0.0862	0.0202	0.1670	-0.0429
TS5	2.006/	C-O	0.2567	0.1706	0.1907	-0.2245	-0.1237	0.3001	-0.2567
TS5a	2.011		0.2537	0.1724	0.1905	-0.2223	-0.1168	0.2924	-0.2537

4. Conclusion

The palladium catalysts are widely utilized for the carbonylation reactions. Ester formation starts from alkene/alkyne, CO, and alcohol and involves methoxycarbonylation. The mechanism consists of the formation of a metal hydride intermediate or alkoxy carbonyl key intermediate. An earlier report suggests the feasibility of the metal hydride intermediate. Previous studies focused on using Pd^{II} catalysts with bidentate diphosphine, NHC-type ligands. The process's final step involves forming an intermolecular transition step at the alcoholysis step and ultimately dictates the mechanism as it involves a high activation energy barrier. Here is the simple starting catalyst [PdCl₂]⁻ formed in situ from PdCl₂ in the presence of HCl. The alkoxy carbonylation of styrene with methanol is considered. The formation of linear ester and branched ester are taken into consideration.

Hence, two cycles are compared side by side in terms of energy. It was shown that the formation of the linear ester is energetically more favorable at the methanolysis step. The novelty of this work stands with the consideration of the alcoholysis step with an entirely new concept. It is hypothesized that the alcohol coordinates to the Pd^{II} center and then undergoes oxidative addition to form hydride, methoxide, and acyl-coordinated five-membered square pyramidal Pd^{IV} intermediate. Next, it undergoes reductive elimination to form the Pd^{II} metal hydride key intermediate and ester. The activation energies for the oxidative addition step are high, while the reductive elimination is very low. Thus, this study introduces another possibility for the alcoholysis step to the alkoxy carbonylation mechanism. The area remains open for research to compare the activation barrier when the Pd catalyst is bonded to other bidentate ancillary ligands based on diphosphine and NHC. Deeper insight into the nature of bonding of the TS structures is gained through the energy decomposition analysis with natural orbital for chemical valence (EDA-NOCV) and quantum theory of atoms in molecules (QTAIM) analysis.

Acknowledgments: PKC would like to thank DST, New Delhi, for the J. C. Bose National Fellowship, grant number SR/S2/JCB-09/2009. SGP thanks the Department of Chemistry, NIT Silchar. We acknowledge the National Supercomputing Mission (NSM) for providing computing resources of 'PARAM Porul' at NIT Trichy, which is implemented by C-DAC and supported by the Ministry of Electronics and Information Technology and Department of Science and Technology (DST), Government of India.

Conflicts of Interest: The authors declare that they have no conflict of interest regarding the publication of this article, financial and/or otherwise.

References

1. Peng, J.-B.; Geng, H.-Q.; Wu, X.-F. The Chemistry of CO: Carbonylation. *Chem* **2019**, *5*, 526–552, doi:10.1016/j.chempr.2018.11.006.
2. Jurado, L.; Posada-Pérez, S.; Axet, M.R. Carbonylation Reactions Using Single-Atom Catalysts. *ChemCatChem* **2024**, doi:10.1002/cctc.202400543.
3. Ma, K.; Martin, B.S.; Yin, X.; Dai, M. Natural product syntheses via carbonylative cyclizations. *Nat. Prod. Rep.* **2019**, *36*, 174–219, doi:10.1039/C8NP00033F.
4. Wu, X.-F.; Fang, X.; Wu, L.; Jackstell, R.; Neumann, H.; Beller, M. Transition-Metal-Catalyzed Carbonylation Reactions of Olefins and Alkynes: A Personal Account. *Acc. Chem. Res.* **2014**, *47*, 1041–1053, doi:10.1021/ar400222k.
5. Beller, M.; Wu, X.-F. *Transition Metal Catalyzed Carbonylation Reactions*; Springer Berlin Heidelberg: Berlin, Heidelberg, 2013; ISBN 978-3-642-39015-9.
6. Wei, W.-M.; Dong, F.-Q.; Zheng, R.-H.; Liu, Y.-Y.; Zhao, T.-T.; Fang, W.-J.; Qin, Y.-D. Theoretical study of the mechanism of palladium-catalyzed hydroaminocarbonylation of styrene with ammonium chloride. *Comput. Theor. Chem.* **2020**, *1191*, 113040, doi:10.1016/j.comptc.2020.113040.
7. Cernak, T.A.; Lambert, T.H. Multicatalytic Synthesis of α -Pyrrolidiny Ketones via a Tandem Palladium(II)/Indium(III)-Catalyzed Aminochlorocarbonylation/Friedel–Crafts Acylation Reaction. *J. Am. Chem. Soc.* **2009**, *131*, 3124–3125, doi:10.1021/ja809897f.
8. Malkov, A. V.; Barlóg, M.; Miller-Potucká, L.; Kabeshov, M.A.; Farrugia, L.J.; Kočovský, P. Stereoselective Palladium-Catalyzed Functionalization of Homoallylic Alcohols: A Convenient Synthesis of Di- and Trisubstituted Isoxazolidines and β -Amino- δ -Hydroxy Esters. *Chem. – A Eur. J.* **2012**, *18*, 6873–6884, doi:10.1002/chem.201102716.
9. Malkov, A. V.; Lee, D.S.; Barlóg, M.; Elsegood, M.R.J.; Kočovský, P. Palladium-Catalyzed Stereoselective Intramolecular Oxidative Amidation of Alkenes in the Synthesis of 1,3- and 1,4-Amino Alcohols and 1,3-Diamines. *Chem. – A Eur. J.* **2014**, *20*, 4901–4905, doi:10.1002/chem.201400123.
10. Wu, X.-F.; Neumann, H.; Beller, M. Synthesis of Heterocycles via Palladium-Catalyzed Carbonylations. *Chem. Rev.* **2013**, *113*, 1–35, doi:10.1021/cr300100s.

11. Kočovský, P.; Bäckvall, J. The syn / anti -Dichotomy in the Palladium-Catalyzed Addition of Nucleophiles to Alkenes. *Chem. – A Eur. J.* **2015**, *21*, 36–56, doi:10.1002/chem.201404070.
12. Shen, C.; Dong, K. Assembling Chiral Center of Heterocycles by Palladium-Catalyzed Asymmetric Hydrocarbonylation. *Synlett* **2022**, *33*, 815–821, doi:10.1055/a-1796-2255.
13. Gallarati, S.; Dingwall, P.; Fuentes, J.A.; Bühl, M.; Clarke, M.L. Understanding Catalyst Structure–Selectivity Relationships in Pd-Catalyzed Enantioselective Methoxycarbonylation of Styrene. *Organometallics* **2020**, *39*, 4544–4556, doi:10.1021/acs.organomet.0c00613.
14. Jing, T.-H.; Zhuang, Y.-Y.; Zhang, X.-X.; Qian, J.-G.; Zhao, X.-L.; Lu, Y.; Wang, H.-J.; Liu, Y. Pinwheel-like tridentate phosphines for controlling divergent regioselectivity in Pd-catalyzed alkoxycarbonylation of alkenes. *J. Catal.* **2024**, *432*, 115406, doi:10.1016/j.jcat.2024.115406.
15. Xu, T.; Sha, F.; Alper, H. Highly Ligand-Controlled Regioselective Pd-Catalyzed Aminocarbonylation of Styrenes with Aminophenols. *J. Am. Chem. Soc.* **2016**, *138*, 6629–6635, doi:10.1021/jacs.6b03161.
16. Li, H.; Dong, K.; Jiao, H.; Neumann, H.; Jackstell, R.; Beller, M. The scope and mechanism of palladium-catalysed Markovnikov alkoxycarbonylation of alkenes. *Nat. Chem.* **2016**, *8*, 1159–1166, doi:10.1038/nchem.2586.
17. Aguirre, P.A.; Lagos, C.A.; Moya, S.A.; Zúñiga, C.; Vera-Oyarce, C.; Sola, E.; Peris, G.; Bayón, J.C. Methoxycarbonylation of olefins catalyzed by palladium complexes bearing P,N-donor ligands. *Dalt. Trans.* **2007**, 5419, doi:10.1039/b704615b.
18. Dai, M.; Wang, C.; Dong, G.; Xiang, J.; Luo, T.; Liang, B.; Chen, J.; Yang, Z. Development of Thiourea-Based Ligands for the Palladium-Catalyzed Bis(methoxycarbonylation) of Terminal Olefins. *European J. Org. Chem.* **2003**, 2003, 4346–4348, doi:10.1002/ejoc.200300543.
19. Fekri, S.; Mansoori, Y. Supported Bis-(NHC)-Pd(II) complex: A phosphine-free catalyst supported on magnetic mesoporous silica for the CO-free carbonylation of aryl halides. *J. Organomet. Chem.* **2024**, *1014*, 123193, doi:10.1016/j.jorganchem.2024.123193.
20. Klingshirn, M.A.; Rogers, R.D.; Shaughnessy, K.H. Palladium-catalyzed hydroesterification of styrene derivatives in the presence of ionic liquids. *J. Organomet. Chem.* **2005**, *690*, 3620–3626, doi:10.1016/j.jorganchem.2005.05.031.
21. Sims, H.S.; Dai, M. Palladium-Catalyzed Carbonylations: Application in Complex Natural Product Total Synthesis and Recent Developments. *J. Org. Chem.* **2023**, *88*, 4925–4941, doi:10.1021/acs.joc.2c02746.
22. Zhang, B.; Yuan, H.; Liu, Y.; Deng, Z.; Douthwaite, M.; Dummer, N.F.; Lewis, R.J.; Liu, X.; Luan, S.; Dong, M.; et al. Ambient-pressure alkoxycarbonylation for sustainable synthesis of ester. *Nat. Commun.* **2024**, *15*, 7837, doi:10.1038/s41467-024-52163-2.
23. Schelwies, M.; Paciello, R.; Pelzer, R.; Siegel, W.; Breuer, M. Palladium-Catalyzed Low Pressure Carbonylation of Allylic Alcohols by Catalytic Anhydride Activation. *Chem. – A Eur. J.* **2021**, *27*, 9263–9266, doi:10.1002/chem.202005324.
24. Fortman, G.C.; Nolan, S.P. N-Heterocyclic carbene (NHC) ligands and palladium in homogeneous cross-coupling catalysis: a perfect union. *Chem. Soc. Rev.* **2011**, *40*, 5151, doi:10.1039/c1cs15088j.
25. Chen, Q.-A.; Ye, Z.-S.; Duan, Y.; Zhou, Y.-G. Homogeneous palladium-catalyzed asymmetric hydrogenation. *Chem. Soc. Rev.* **2013**, *42*, 497–511, doi:10.1039/C2CS35333D.
26. Roberts, G.M.; Pierce, P.J.; Woo, L.K. Palladium Complexes with N-Heterocyclic Carbene Ligands As Catalysts for the Alkoxycarbonylation of Olefins. *Organometallics* **2013**, *32*, 2033–2036, doi:10.1021/om300959f.
27. Demir, S.; Özdemir, İ.; Arslan, H.; VanDerveer, D. Butylene linked palladium N-heterocyclic carbene complexes: Synthesis and catalytic properties. *J. Organomet. Chem.* **2011**, *696*, 2589–2593, doi:10.1016/j.jorganchem.2011.03.040.
28. Brennfürer, A.; Neumann, H.; Beller, M. Palladium-Catalyzed Carbonylation Reactions of Aryl Halides and Related Compounds. *Angew. Chemie Int. Ed.* **2009**, *48*, 4114–4133, doi:10.1002/anie.200900013.
29. Flahaut, A.; Roland, S.; Mangeney, P. Allylic alkylation and amination using mixed (NHC)(phosphine) palladium complexes under biphasic conditions. *J. Organomet. Chem.* **2007**, *692*, 5754–5762, doi:10.1016/j.jorganchem.2007.10.012.
30. Hashmi, A.S.K.; Lothschütz, C.; Döpp, R.; Rudolph, M.; Ramamurthi, T.D.; Rominger, F. Gold and Palladium Combined for Cross-Coupling. *Angew. Chemie Int. Ed.* **2009**, *48*, 8243–8246, doi:10.1002/anie.200902942.
31. Amatore, C.; Carre, E.; Jutand, A.; M'Barki, M.A. Rates and Mechanism of the Formation of Zerovalent Palladium Complexes from Mixtures of Pd(OAc)₂ and Tertiary Phosphines and Their Reactivity in Oxidative Additions. *Organometallics* **1995**, *14*, 1818–1826, doi:10.1021/om00004a039.
32. Tooze, R.P.; Whiston, K.; Malyan, A.P.; Taylor, M.J.; Wilson, N.W. Evidence for the hydride mechanism in the methoxycarbonylation of ethene catalysed by palladium–triphenylphosphine complexes. *J. Chem. Soc. Dalt. Trans.* **2000**, 3441–3444, doi:10.1039/b005232i.
33. Nguyen, D.H.; Laurenczy, G.; Urrutigoity, M.; Kalck, P. Hydride Route for the Palladium-Catalysed Cyclocarbonylation of Monoterpenes. *Eur. J. Inorg. Chem.* **2005**, 2005, 4215–4225, doi:10.1002/ejic.200500136.

34. Mehara, J.; Anania, M.; Kočovský, P.; Roithová, J. Competing Mechanisms in Palladium-Catalyzed Alkoxy carbonylation of Styrene. *ACS Catal.* **2024**, *14*, 5710–5719, doi:10.1021/acscatal.4c00966.
35. Seayad, A.; Jayasree, S.; Damodaran, K.; Toniolo, L.; Chaudhari, R.V. On the mechanism of hydroesterification of styrene using an in situ-formed cationic palladium complex. *J. Organomet. Chem.* **2000**, *601*, 100–107, doi:10.1016/S0022-328X(00)00041-3.
36. Eastham, G.R.; Tooze, R.P.; Heaton, B.T.; Iggo, J.A.; Whyman, R.; Zacchini, S. Synthesis and spectroscopic characterisation of all the intermediates in the Pd-catalysed methoxycarbonylation of ethene. *Chem. Commun.* **2000**, 609–610, doi:10.1039/b001110j.
37. Muñoz, B.K.; Santos Garcia, E.; Godard, C.; Zangrando, E.; Bo, C.; Ruiz, A.; Claver, C. HP-NMR Study of the Pd-Catalyzed Methoxycarbonylation of Styrene Using Monodentate and Bidentate Phosphane-Modified Systems. *Eur. J. Inorg. Chem.* **2008**, *2008*, 4625–4637, doi:10.1002/ejic.200800502.
38. Bianchini, C.; Meli, A.; Oberhauser, W.; Parisel, S.; Gusev, O. V.; Kal'sin, A.M.; Vologdin, N. V.; Dolgushin, F.M. Methoxycarbonylation of styrene to methyl arylpropanoates catalyzed by palladium(II) precursors with 1,1'-bis(diphenylphosphino)metallocenes. *J. Mol. Catal. A Chem.* **2004**, *224*, 35–49, doi:10.1016/j.molcata.2004.06.029.
39. Clegg, W.; Eastham, G.R.; Elsegood, M.R.J.; Heaton, B.T.; Iggo, J.A.; Tooze, R.P.; Whyman, R.; Zacchini, S. Characterization and Dynamics of $[Pd(L-L)H(solvent)] +$, $[Pd(L-L)(CH_2CH_3)] +$, and $[Pd(L-L)(C(O)Et)(THF)] +$ (L-L = 1,2-(CH₂PBu_t)₂C₆H₄): Key Intermediates in the Catalytic Methoxycarbonylation of Ethene to Methylpropanoate. *Organometallics* **2002**, *21*, 1832–1840, doi:10.1021/om010938g.
40. Naire, R.; Chenal, T.; Ciprés, I.; Kalck, P.; Daran, J.-C.; Vaissermann, J. Carbon monoxide as a building block in organic synthesis. Part V. Involvement of palladium-hydride species in carbonylation reactions of monoterpenes. X-ray crystal structure of $[Ph_3PCH_2CH_2CHPh]_4[PdCl_6][SnCl_6]$. *J. Organomet. Chem.* **1994**, *480*, 91–102, doi:10.1016/0022-328X(94)87106-X.
41. Eastham, G.R.; Tooze, R.P.; Kilner, M.; Foster, D.F.; Cole-Hamilton, D.J. Deuterium labelling evidence for a hydride mechanism in the formation of methyl propanoate from carbon monoxide, ethene and methanol catalysed by a palladium complex. *J. Chem. Soc. Dalt. Trans.* **2002**, 1613–1617, doi:10.1039/b201514e.
42. Liu, J.; Heaton, B.T.; Iggo, J.A.; Whyman, R.; Bickley, J.F.; Steiner, A. The Mechanism of the Hydroalkoxy carbonylation of Ethene and Alkene-CO Copolymerization Catalyzed by Pd II-Diphosphine Cations. *Chem. – A Eur. J.* **2006**, *12*, 4417–4430, doi:10.1002/chem.200501398.
43. Amadio, E.; Cavinato, G.; Dolmella, A.; Toniolo, L. Catalytic Properties of $[Pd(COOMe)_nX_{2-n}(PPh_3)_2]$ (n = 0, 1, 2; X = Cl, NO₂, ONO₂, OAc and OTs) in the Oxidative Carbonylation of MeOH. *Inorg. Chem.* **2010**, *49*, 3721–3729, doi:10.1021/ic901569w.
44. Malkov, A. V.; Derrien, N.; Barlóg, M.; Kočovský, P. Palladium-Catalyzed Alkoxy carbonylation of Terminal Alkenes To Produce α,β -Unsaturated Esters: The Key Role of Acetonitrile as a Ligand. *Chem. – A Eur. J.* **2014**, *20*, 4542–4547, doi:10.1002/chem.201304798.
45. Ahmad, S.; Bühl, M. Computational modelling of Pd-catalysed alkoxy carbonylation of alkenes and alkynes. *Phys. Chem. Chem. Phys.* **2021**, *23*, 15869–15880, doi:10.1039/D1CP02426D.
46. van Leeuwen, P.W.N.M.; Zuideveld, M.A.; Swennenhuis, B.H.G.; Freixa, Z.; Kamer, P.C.J.; Goubitz, K.; Fraanje, J.; Lutz, M.; Spek, A.L. Alcoholysis of Acylpalladium(II) Complexes Relevant to the Alternating Copolymerization of Ethene and Carbon Monoxide and the Alkoxy carbonylation of Alkenes: the Importance of Cis-Coordinating Phosphines. *J. Am. Chem. Soc.* **2003**, *125*, 5523–5539, doi:10.1021/ja029341y.
47. Clegg, W.; Eastham, G.R.; Elsegood, M.R.J.; Heaton, B.T.; Iggo, J.A.; Tooze, R.P.; Whyman, R.; Zacchini, S. Synthesis and reactivity of palladium hydrido-solvento complexes, including a key intermediate in the catalytic methoxycarbonylation of ethene to methyl propanoate. *J. Chem. Soc. Dalt. Trans.* **2002**, 3300–3308, doi:10.1039/b202372p.
48. Ahmad, S.; Crawford, L.E.; Bühl, M. Palladium-catalysed methoxycarbonylation of ethene with bidentate diphosphine ligands: a density functional theory study. *Phys. Chem. Chem. Phys.* **2020**, *22*, 24330–24336, doi:10.1039/D0CP04454G.
49. Frisch, M.J.; Trucks, G.W.; Schlegel, H. B.; Scuseria, G.E.; Robb, M. A.; Cheeseman, J. R.; Scalmani, G.; Barone, V.; Petersson, G. A.; Nakatsuji, H.; Li, X.; Caricato, M.; Marenich, A.V.; Bloino, J.; et al. Gaussian 16, Revision C.01 2016.
50. Ernzerhof, M.; Scuseria, G.E. Assessment of the Perdew–Burke–Ernzerhof exchange–correlation functional. *J. Chem. Phys.* **1999**, *110*, 5029–5036, doi:10.1063/1.478401.
51. Adamo, C.; Barone, V. Toward reliable density functional methods without adjustable parameters: The PBE0 model. *J. Chem. Phys.* **1999**, *110*, 6158–6170, doi:10.1063/1.478522.
52. Hay, P.J.; Wadt, W.R. Ab initio effective core potentials for molecular calculations. Potentials for K to Au including the outermost core orbitals. *J. Chem. Phys.* **1985**, *82*, 299–310, doi:10.1063/1.448975.
53. Dolg, M.; Stoll, H.; Preuss, H.; Pitzer, R.M. Relativistic and correlation effects for element 105 (hahnium, Ha): a comparative study of M and MO (M = Nb, Ta, Ha) using energy-adjusted ab initio pseudopotentials. *J. Phys. Chem.* **1993**, *97*, 5852–5859, doi:10.1021/j100124a012.

54. Bergner, A.; Dolg, M.; Küchle, W.; Stoll, H.; Preuß, H. Ab initio energy-adjusted pseudopotentials for elements of groups 13–17. *Mol. Phys.* **1993**, *80*, 1431–1441, doi:10.1080/00268979300103121.
55. Marenich, A. V.; Cramer, C.J.; Truhlar, D.G. Universal Solvation Model Based on Solute Electron Density and on a Continuum Model of the Solvent Defined by the Bulk Dielectric Constant and Atomic Surface Tensions. *J. Phys. Chem. B* **2009**, *113*, 6378–6396, doi:10.1021/jp810292n.
56. Martin, R.L.; Hay, P.J.; Pratt, L.R. Hydrolysis of Ferric Ion in Water and Conformational Equilibrium. *J. Phys. Chem. A* **1998**, *102*, 3565–3573, doi:10.1021/jp980229p.
57. Sparta, M.; Riplinger, C.; Neese, F. Mechanism of Olefin Asymmetric Hydrogenation Catalyzed by Iridium Phosphino-Oxazoline: A Pair Natural Orbital Coupled Cluster Study. *J. Chem. Theory Comput.* **2014**, *10*, 1099–1108, doi:10.1021/ct400917j.
58. Fantuzzi, F.; Nascimento, M.A.C.; Ginovska, B.; Bullock, R.M.; Raugei, S. Splitting of multiple hydrogen molecules by bioinspired diniobium metal complexes: a DFT study. *Dalt. Trans.* **2021**, *50*, 840–849, doi:10.1039/D0DT03411H.
59. Lu, T.; Chen, F. Multiwfn: A multifunctional wavefunction analyzer. *J. Comput. Chem.* **2012**, *33*, 580–592, doi:10.1002/jcc.22885.
60. Lu, T.; Chen, Q. Simple, Efficient, and Universal Energy Decomposition Analysis Method Based on Dispersion-Corrected Density Functional Theory. *J. Phys. Chem. A* **2023**, *127*, 7023–7035, doi:10.1021/acs.jpca.3c04374.
61. Grimme, S.; Antony, J.; Ehrlich, S.; Krieg, H. A consistent and accurate ab initio parametrization of density functional dispersion correction (DFT-D) for the 94 elements H–Pu. *J. Chem. Phys.* **2010**, *132*, 154104, doi:10.1063/1.3382344.
62. Grimme, S.; Ehrlich, S.; Goerigk, L. Effect of the damping function in dispersion corrected density functional theory. *J. Comput. Chem.* **2011**, *32*, 1456–1465, doi:10.1002/jcc.21759.
63. Walther, G.; Knöpke, L.R.; Rabeah, J.; Chęciński, M.P.; Jiao, H.; Bentrup, U.; Brückner, A.; Martin, A.; Köckritz, A. From sunflower oil toward 1,19-diester: Mechanistic elucidation. *J. Catal.* **2013**, *297*, 44–55, doi:10.1016/j.jcat.2012.09.016.
64. Roesle, P.; Caporaso, L.; Schnitte, M.; Goldbach, V.; Cavallo, L.; Mecking, S. A Comprehensive Mechanistic Picture of the Isomerizing Alkoxycarbonylation of Plant Oils. *J. Am. Chem. Soc.* **2014**, *136*, 16871–16881, doi:10.1021/ja508447d.
65. Dong, K.; Sang, R.; Wei, Z.; Liu, J.; Dühren, R.; Spannenberg, A.; Jiao, H.; Neumann, H.; Jackstell, R.; Franke, R.; et al. Cooperative catalytic methoxycarbonylation of alkenes: uncovering the role of palladium complexes with hemilabile ligands. *Chem. Sci.* **2018**, *9*, 2510–2516, doi:10.1039/C7SC02964K.
66. Gopal Patra, S.; Kumar Chattaraj, P. Three coordinated first row-transition metal complexes, [M{N(SiMe₃)₂}₃]-1/0: Structure, bonding, and magnetic properties. *Polyhedron* **2024**, *256*, 116990, doi:10.1016/j.poly.2024.116990.
67. Pal, R.; Patra, S.G.; Chattaraj, P.K. Can a chemical bond be exclusively covalent or ionic? *J. Chem. Sci.* **2022**, *134*, 108, doi:10.1007/s12039-022-02094-6.
68. Patra, S.G.; Drew, M.G.B.; Datta, D. δ -Acidity of benzene in [(benzene)RuII(N–N)Cl]⁺. Crystal structures, nuclear magnetic resonance spectra and nucleus independent chemical shifts. *Inorganica Chim. Acta* **2018**, *471*, 228–233, doi:10.1016/j.ica.2017.10.025.
69. Bader, R.F.W. Atoms in molecules. *Acc. Chem. Res.* **1985**, *18*, 9–15, doi:10.1021/ar00109a003.
70. Bader, R.F.W.; Essén, H. The characterization of atomic interactions. *J. Chem. Phys.* **1984**, *80*, 1943–1960, doi:10.1063/1.446956.
71. Bader, R.F.W. A Bond Path: A Universal Indicator of Bonded Interactions. *J. Phys. Chem. A* **1998**, *102*, 7314–7323, doi:10.1021/jp981794v.
72. R.F.W. Bader *Atoms in Molecules, A Quantum Theory*; Oxford University Press: Oxford, 1990;

Disclaimer/Publisher's Note: The statements, opinions and data contained in all publications are solely those of the individual author(s) and contributor(s) and not of MDPI and/or the editor(s). MDPI and/or the editor(s) disclaim responsibility for any injury to people or property resulting from any ideas, methods, instructions or products referred to in the content.